Experimental and Theoretical Study of Periodic Intensity Bursts in the Start-Up Phase of a Free-Electron Laser Oscillator

Eli Jerby, George Bekefi, and Jonathan S. Wurtele

Abstract—**Experimental observations and a theoretical analysis of periodic radiation bursts and macropulse formation in the start-up phase of a free-electron laser (FEL) oscillator are presented. This microwave FEL uses a long pulse electron beam with a slowly decaying voltage. The output radiation consists of a superposition of bell-shaped macropulses, each of which is composed of a periodic sequence of short micropulses. The micropulses are separated by a cavity round-trip time. Each bell-shaped macropulse has a random start-up time and amplitude. The startup of the radiation macropulses is correlated with random current spikes on the continuous electron beam. The observed macropulse signal agrees with a theoretical calculation of the impulse response of the FEL oscillator when the shift in the FEL resonance frequency arising from the slow voltage drop of the electron beam is included in the analysis. Possible applications of the macropulse formation phenomena in the FEL are discussed.**

I. Introduction

THIS paper presents new experimental observations of the spontaneous excitation of periodic radiation bursts and macropulse formation in the start-up phase of a free-electron laser (FEL) oscillator. The radiation pulse consists of a superposition of bell-shaped macropulses each of which is composed of a sequence of short-pulse micropulses. The micropulses within a given macropulse are separated by a cavity round-trip time. The amplitude of the micropulses has the bell-shaped macropulse structure. The structure of a macropulse, including micropulse width and separation and the bell-shaped envelope, is described by a linear model of the impulse response of the FEL oscillator.

Mechanisms of micropulse formation have been studied in a wide variety of fields, such as microwave tubes, conventional lasers, and FEL's. In most cases micropulse formation is related to nonlinear phenomena, such as mode locking or solitons. Narrow microwave pulses were produced in the early fifties with regenerative oscillators. One such short-pulse generator was constructed as a closed loop of a traveling wave tube (TWT) amplifier, a filter, and a nonlinear pulse expander [1]. It produced microwave micropulses of ~ 2 ns width. Short pulse phenomena in conventional atomic and molecular lasers have been studied intensively in the last two decades. These include the nonlinear phenomenon of self (spontaneous) spiking [2], as well as a wide range of mode-locking mechanisms [3], and soliton formation [4].

In FEL's, radiation bursts or spikes, as they are often called, have been studied experimentally and theoretically in the nonlinear regime by several groups [5]–[11]. The appearance of radiation spikes in the FEL nonlinear regime is caused by the sideband instability which, in turn, is driven by electron oscillations in the potential well of the ponderomotive wave. In contrast, our studies [13] deal with the buildup of short electromagnetic radiation bursts that occur well before saturation and near oscillation threshold, where linear phenomena dominate the interaction.

Numerous theoretical and experimental investigations of phenomena related to radiation bursts are found in the literature. These include studies of noise in FEL amplifiers [14], spontaneous emission and coherence buildup [15], self-amplification of spontaneous emission [16], prebunching [17], [18], slippage and superradiance [19], [20], effects of electron energy drift [21], mode competition [22], phase locking [23], spectral analysis [24], and pulse compression [25].

This paper is organized as follows: In Section II we describe the experimental system and results. In Section III, we utilize the linear analysis of the prebunched FEL amplifier to evaluate the impulse response of a multipass FEL oscillator. The model includes the slow voltage droop on the electron beam, and the competition of waveguide losses and dispersion with FEL gain and dispersion. The radiation from an initially localized density perturbation, calculated in the time domain over many passes through the wiggler, agrees with the experimentally observed macropulse structure. A discussion of the macropulse formation in FEL oscillators and some possible applications is presented in Section IV.

Manuscript received April 16, 1991; revised June 26, 1991.

E. Jerby is with the Department of Physics, Research Laboratory of Electronics and Plasma Fusion Center, Massachusetts Institute of Technology, Cambridge, MA 02139, on leave from the Faculty of Engineering, Tel Aviv University, Ramat Aviv 69978, Israel.

G. Bekefi and J. S. Wurtele are with the Department of Physics, Research Laboratory of Electronics and Plasma Fusion Center, Massachusetts Institute of Technology, Cambridge, MA 02139.

IEEE Log Number 9103684.

II. The FEL Oscillator Experiment

The microwave FEL oscillator employs a long pulse low-energy electron beam. In its start-up phase, the oscillator emits periodic short RF micropulses in bell-shaped envelopes. The experimental apparatus is described in Section II-A, and the experimental observations are presented in Section II-B.

A. Experimental Configuration

The experimental setup is shown schematically in Fig. 1. A microwave FEL amplifier [24], [25] was converted to operate as an FEL oscillator by eliminating the input signal and feeding the microwave output power back to the wiggler entrance.

The accelerating voltage is supplied by a Marx generator (Physics International Pulserad 615 MR) without a pulse forming network. The voltage decays exponentially, due to the Marx *RC* droop, as

$$V_{eb}(t) = V_0 \exp(-t/\tau_m) \tag{1}$$

where $V_0 \cong 0.2$ MV is the initial Marx voltage and $\tau_m \cong 25$ μs is the time constant of the Marx *RC* circuit.

The electron beam is generated by a thermionically emitting, electrostatically focused, Pierce-type electron gun (250 kV, 250 A) from a SLAC klystron (Model 343). An emittance selector limits the beam current to ~ 1 A.

The electron beam is transported into the rectangular stainless steel drift tube by an assembly of focusing coils. The beam is confined in the FEL region by a uniform 1.6 kG axial magnetic field produced by a solenoid, and the FEL coupling is generated by a bifilar helical wiggler. The 65 period wiggler has period $\lambda_w = 3.5$ cm and field amplitude $B_w = 200$–400 G. An aperture limits the size of the beam to $r_b \simeq 0.07\lambda_w$, so that the wiggler field appears nearly sinusoidal to the drifting electrons. A slowly increasing field amplitude taper is produced at the wiggler entrance by resistively loading the first six periods of the wiggler.

The 2.7 m long drift tube acts as a rectangular waveguide for the electromagnetic radiation. Its inner dimensions are $0.90'' \times 0.40''$ and the fundamental TE_{10} mode has a cutoff frequency of 6.6 GHz. The waveguide closes upon itself, thereby forming a ring cavity 7.6 m in length, as shown in Fig. 1. The system is operated in a frequency range between 8 and 11 GHz. At these frequencies, the empty waveguide can support only the fundamental (TE_{10}) mode, all higher modes being evanescent. The ring cavity loss is 5.5 dB and the single-pass FEL gain varies between 6 and 8.5 dB, so that the overall system gain is less than 3 dB. It is in this low net gain operating regime, where the periodic RF spikes are the clearest, that all of our measurements are carried out.

The radiation field in the ring cavity is sampled by means of a 20 dB directional coupler. In some of our measurements the sampled signal passes through a band-pass filter (9.6–10.2 GHz) or a high-pass filter (9.6 GHz). The radiation power is measured with a calibrated crystal detector.

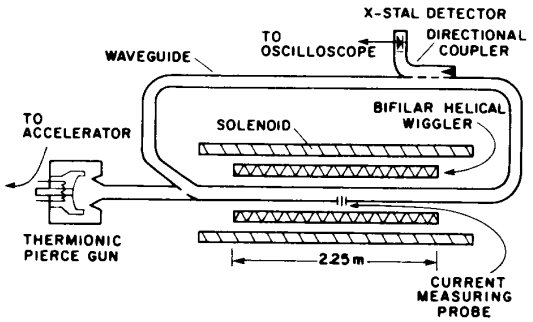

Fig. 1. The experimental setup of the FEL oscillator.

B. Experimental Observations

The FEL oscillator emits bursts of microwave radiation. Fig. 2(a) shows the full RF signal during one shot, and Fig. 2(b) shows, on the same time scale as Fig. 2(a), the Marx voltage droop. Radiation bursts typically start ~ 7 μs after the Marx ignition and completely disappear ~ 2 μs later.

Fig. 3 shows a typical radiation burst in greater detail. The pulse appears noisy and irregular, though some periodic structures can be identified. The underlying temporal structure is revealed by filtering the microwave signal with a band-pass filter placed in the output arm of the directional coupler. Fig. 4 shows the radiation bursts detected through a 9.6–10.2 GHz band-pass filter. The filtered pulse is seen to be composed of a sequence of partially overlapping bell-shaped macropulses with random start-up times and amplitudes. Each macropulse consists of a series of micropulses within a bell-shaped envelope. (As will be discussed below, the bell-shaped envelope results from the voltage droop of the electron beam). The micropulse width (FWHM) is ~ 5 ns, and no significant broadening is observed over many round-trips. The distance between two successive micropulses in Fig. 4 is ~ 36 ns. This corresponds to the roundtrip time of an RF micropulse, with a center frequency of $f_0 \cong 9.6$ GHz, in the 7.6 m ring cavity. Increasing the cavity length to 11.3 m results in a similar bell-shaped macropulses with a longer period (51 ns) between the micropulses. The micropulse period is again in agreement with the RF roundtrip time (in the 11.3 m cavity).

In all the runs performed (totalling over 100), bell-shaped macropulses are seen to be the underlying building blocks of the radiation bursts. The macropulses are most easily observed when the FEL is operated just above oscillation threshold. As the gain is increased, the density of macropulses increases and individual macropulses become harder to distinguish. The number of macropulses in a burst varies randomly from one run to another. Similar bell-shaped macropulses are observed when the filter is moved from the output coupler and placed in the return leg of the ring cavity.

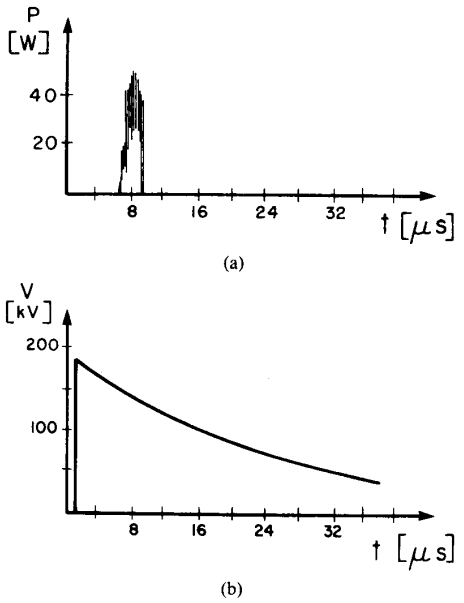

Fig. 2. (a) The unfiltered RF bursts, and (b) the Marx accelerator *RC* voltage droop (on the same time scale).

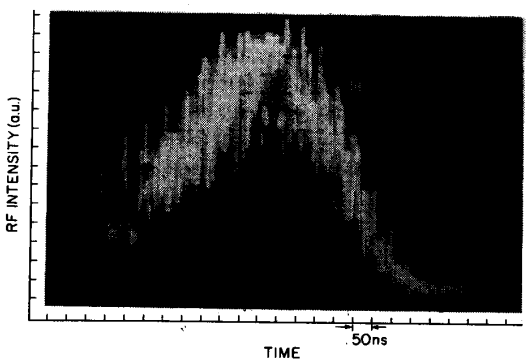

Fig. 3. Typical unfiltered RF bursts.

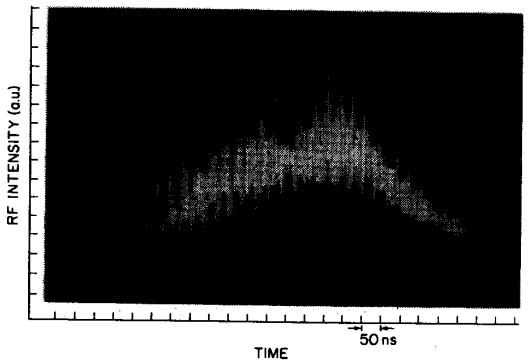

Fig. 4. RF bursts filtered by a band-pass filter, $f = 9.6$–10.2 GHz.

The random start-up times of the macropulses and their appearance are correlated to spikes in the current density. Fig. 5 shows the electron beam current density measured

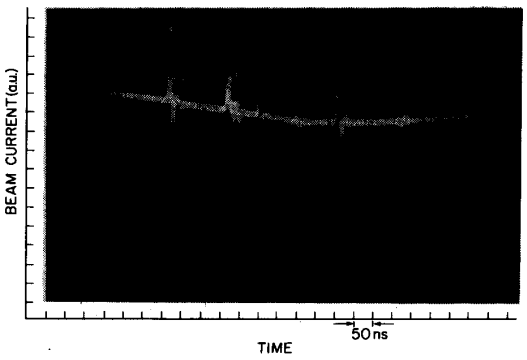

Fig. 5. Random spikes in the electron beam current.

by a tiny probe [26] which is partially inserted into the electron beam. The probe is placed ~1 m from the beginning of the wiggler. The random current spikes are clearly seen superposed on the dc current. The width of the current spikes (FWHM), measured by a fast transient recorder (Tektronix SCD 1000), was found to be typically narrower than 1 ns.

The radiation bursts and the electron beam current were recorded simultaneously using a LeCroy 7200 two-channel digital oscilloscope with a 1 GHz sampling rate. This enabled us to make a detailed analysis of the RF intensity, the current fluctuations, and any correlations between their temporal structures. In these measurements, in order to reduce the micropulse broadening, we replaced the band-pass filter with a high pass filter ($f > 9.6$ GHz).

Fig. 6(a) shows a typical example of the radiation bursts on an expanded scale. Two dominant macropulses with partially overlapping bell-shaped envelopes, marked as A and B, are clearly seen. Each macropulse consists of a series of micropulses. The micropulse period is 32 ns in macropulse A, and 34 ns in B. The micropulse width is ~5 ns for both macropulses, and no significant broadening is observed in successive round-trips.

Fig. 6(b) shows the simultaneous electron beam current, and the random spikes associated with it, on the same time scale as Fig. 6(a). The first two current spikes are marked in Fig. 6(b) as A′ and B′. The time between the current spike A′ and the peak of macropulse A is 516 ns, and the time between the current spike B′ and the peak of macropulse B is 510 ns. The relation between these current spikes and the radiation pulses in Fig. 6(a) is developed in the next section.

III. A Time Domain Analysis of the FEL Oscillator

The periodic radiation bursts and macropulse formation presented in the previous section are observed well before saturation, i.e., in the small-signal regime. Therefore, we can apply a small-signal linear theory to analyze these phenomena. In Section III-A, we review the linear model of the prebunched FEL amplifier in the frequency and time domains. In Section III-B, we extend the model to de-

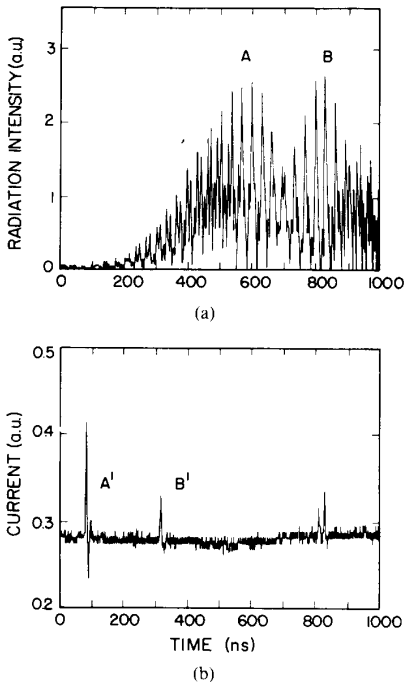

Fig. 6. (a) The RF output bursts filtered by a high-pass filter, $f > 9.6$ GHz, and (b) the associated spikes of the electron beam current. Both signals were recorded simultaneously by a fast digital oscilloscope (LeCroy 7200).

scribe the FEL oscillator in the time domain. The impulse response of the FEL oscillator is computed and compared to the RF macropulses observed in the experiment.

A. Amplification, Prebunching, and Spontaneous Emission

Electromagnetic radiation in an FEL is generated by various mechanisms, such as spontaneous emission from single electrons [15], signal amplification [27], a prebunched electron beam [17], [18], and the self-amplification of spontaneous emission [16]. These mechanisms are distinguished by the source of excitation which initiates the radiation. In the amplification process, the radiation is stimulated by the injection of an input field at the FEL resonant frequency. The prebunched FEL is excited by an initial modulation of the electron beam distribution at the resonant frequency. In the spontaneous emission process, the emission of radiation is induced by random velocity and density fluctuations in the electron beam. Typically, the sources of RF noise are spread over a wide frequency spectrum, including the resonance band in which FEL radiation is excited. All these phenomena are described by transfer functions which relate the output radiation to the excitation sources, namely the input field and the non-uniform electron beam distribution at the wiggler entrance.

In the FEL amplification process, the relation between the output field, $\tilde{\bar{E}}_o(i\delta k, \omega)$, and the input field, $\tilde{\bar{E}}_i(\omega)$, is given, for a cold beam, in wavenumber-frequency space, by the gain-dispersion equation [27], [28]:

$$\tilde{\bar{E}}_o(i\delta k, \omega) = \frac{(\delta k - \theta)^2 - \theta_p^2}{i\delta k[(\delta k - \theta)^2 - \theta_p^2] + i\kappa\theta_p^2} \tilde{\bar{E}}_i(\omega) \quad (2)$$

where ω is the wave frequency, and δk is the complex modification (due to the FEL interaction) to k_z, the axial wavenumber of the mode in vacuum. With this notation, the Laplace transform variable is $s = ik_z + i\delta k$, and $\bar{a}(s) = L\{a(z)\} = \int_z a(z)\, e^{-sz}\, dz$.

The FEL parameters θ_p, κ, and $\bar{\theta}$ are related to physical quantities. The space-charge parameter θ_p is

$$\theta_p = \sqrt{\frac{e^2 n_0}{\gamma\gamma_z^2 \epsilon_0 m V_z^2}} \quad (3)$$

where e is the electron charge, m is the electron mass, n_0 is the electron beam density, V_z is the axial beam velocity, γ is the beam energy in units of mc^2, $\gamma_z = \sqrt{1/(1 - \beta_z^2)}$, $\beta_z = V_z/c$, and ϵ_0 is the permittivity of free space. The coupling parameter κ and the gain parameter Q are

$$\kappa = \frac{1}{4}\frac{\omega}{V_z}\left(\frac{\bar{V}_\perp}{c}\right)^2 \qquad Q = \kappa\theta_p^2 \quad (4a) \text{ and } (4b)$$

where $\bar{V}_\perp$ is the amplitude of the perpendicular component of the electron velocity. The detuning parameter $\bar{\theta}$ is defined by

$$\bar{\theta} = \theta L_w = \left(\frac{\omega}{V_z} - k_z - k_w\right) L_w \quad (5)$$

where $L_w = N_w \lambda_w$ is the wiggler length and $k_w = 2\pi/\lambda_w$.

For both spontaneous emission and an initial prebunching of the electron beam, the FEL output field is excited by an initially nonuniform electron beam distribution. The relations between the output field, $\tilde{\bar{E}}_o(i\delta k, \omega)$, and the ac input density component $\tilde{n}_i(\omega)$ and velocity component, $\tilde{v}_i(\omega)$, are given [17], [29] by

$$\tilde{\bar{E}}_o(i\delta k, \omega) = -i\alpha_n \frac{(\delta k - \theta)}{D(i\delta k, \omega)} \tilde{n}_i(\omega) \quad (6a)$$

and

$$\tilde{\bar{E}}_o(i\delta k, \omega) = -i\alpha_{v} \frac{(k_z + k_w)}{D(i\delta k, \omega)} \tilde{v}_i(\omega) \quad (6b)$$

respectively, where the coefficients α_n and α_v are

$$\alpha_n = \frac{1}{4} eZ_0 V_\perp \qquad \alpha_v = \frac{1}{4} en_0 Z_0 \frac{V_\perp}{V_z} \quad (7a) \text{ and } (7b)$$

$Z_0 = 377\ \Omega$ is the impedance of free space, and $D(i\delta k, \omega)$ is the denominator of (2),

$$D(i\delta k, \omega) = i\delta k[(\delta k - \theta)^2 - \theta_p^2] + i\kappa\theta_p^2. \quad (8)$$

Equations (6a) and (6b) apply to a prebunched electron beam whose ac components, $\tilde{n}_i(\omega)$ and $\tilde{v}_i(\omega)$, are at the same frequency as the RF output signal. These relations can be extended to describe shot noise and other types of

random fluctuations in which the electron beam distribution is defined by statistical features such as its spectral power density.

The transfer functions (2), (6a), and (6b) are given in Laplace–Fourier space $(i\delta k, \omega)$. In order to find the spectral transfer functions between the output radiation at the wiggler exit $z = L_w$, $\tilde{E}_o(\omega)$, and each of the input excitations $[\tilde{E}_i(\omega)$, $\tilde{n}_i(\omega)$, and $\tilde{v}_i(\omega)]$ at $z = 0$, we must perform an inverse Laplace transform on the transfer functions.

The FEL dispersion equation [the denominator of (2)]

$$D(i\delta k_m, \omega) = 0 \tag{9}$$

is a Pierce-type cubic equation [30]. The zeroes δk_m $(m = 1, 2, 3)$ of the cubic dispersion (9) are found numerically. The residues of (2), (6a), and (6b) are denoted as R_m^E, R_m^n, and R_m^v, respectively. The residues of (2), for instance, are given by

$$R_m^E = \left[\frac{(\delta k - \theta)^2 - \theta_p^2}{i\delta k[(\delta k - \theta)^2 - \theta_p^2] + i\kappa\theta_p^2} \cdot (\delta k - \delta k_m)\right]_{\delta k = \delta k_m} \tag{10}$$

for $m = 1, 2, 3$. Similarly, the residues of (6a) are $R_m^n = [-i\alpha_n(\delta k - \theta)(\delta k - \delta k_m)/D(i\delta k, \omega)]_{\delta k = \delta k_m}$, and the residues of (6b) are $R_m^v = [-j\alpha_v(k_z + k_w)(\delta k - \delta k_m)/D(i\delta k, \omega)]_{\delta k = \delta k_m}$.

With the above definitions, the spectral transfer functions between $\tilde{E}_o(\omega)$ and each of the inputs are given by the inverse Laplace transform as

$$T_E(\omega) = \sum_{m=1}^{3} R_m^E e^{s_m L_w} \tag{11a}$$

$$T_n(\omega) = \sum_{m=1}^{3} R_m^n e^{s_m L_w} \tag{11b}$$

$$T_v(\omega) = \sum_{m=1}^{3} R_m^v e^{s_m L_w} \tag{11c}$$

where $s_m = i\delta k_m + ik_z$ are the poles in the complex s plane. Fig. 7 shows the amplitude curves of the FEL gain, $T_E(\omega)$, and the prebunched FEL emission $T_n(\omega)$ for the parameters of our experiment. (The latter curve corresponds also to the FEL spontaneous emission for a uniform spectral density of the electron fluctuations, $|n_i(\omega)|^2 = \text{const.}$).

The total output field is then given by the superposition

$$\tilde{E}_o(\omega) = T_E(\omega)\tilde{E}_i(\omega) + T_n(\omega)\tilde{n}_i(\omega) + T_v(\omega)\tilde{v}_i(\omega) \tag{12}$$

and the corresponding output spectral power density is given by $|\tilde{E}_o(\omega)|^2$.

In the time domain, the FEL *impulse response* functions are obtained [31] by performing the inverse Fourier transform of (11a), (11b), and (11c). For instance, the response function to a density impulse in the electron beam is given by

$$h_n(\tau) = F^{-1}\{T_n(\omega)\} = \frac{1}{2\pi}\int_t T_n(\omega)\, e^{-i\omega\tau}\, d\omega. \tag{13}$$

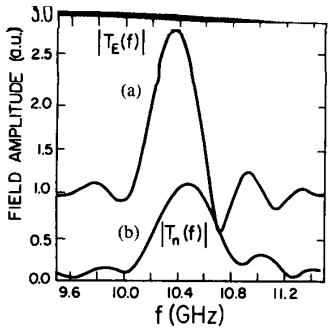

Fig. 7. (a) The FEL gain curve $|T_E(f)|$, and (b) the prebunched FEL emission curve $|T_n(f)|$, computed from (11a) and (11b), respectively, for our experimental parameters.

The function $h_n(\tau)$ gives the output field $E_o(\tau)$ due to an impulse electron density $n(\tau) = \delta(\tau)$. Similar integrals define the responses to an input field impulse, $h_E(\tau) = F^{-1}\{T_E(\omega)\}$, and to a velocity impulse, $h_v(\tau) = F^{-1}\{T_v(\omega)\}$. Fig. 8 shows the amplitude of the impulse response function $h_n(\tau)$ for the parameters of our experiment. The output field produced by an electron current impulse at $t = 0$ is seen to be a delayed pulse with a finite width.

The impulse response $h_n(\tau)$ can be found analytically in the limit of weak coupling, low-gain $(\bar{Q} = \kappa\theta_p^2 L_w < 1)$, and a tenuous electron beam $(\bar{\theta}_p = \theta_p L_w < \pi)$. Though our FEL operates in the intermediate high-gain regime, and we use numerical methods to analyze it, analytic solutions in the low-gain limit can provide physical insight.

The dispersion (9) has a simple solution in the low-gain limit. The prebunched FEL equation (6a) can be expanded to first order in Q, as

$$\tilde{E}_o(i\delta k, \omega) = \{D_0(i\delta k, \omega)^{-1} - D_0(i\delta k, \omega)^{-2} \cdot Q\} \cdot -i\alpha_n(\delta k - \theta)\tilde{n}_i \tag{14}$$

where the zero-order dispersion equation, in this limit, is $D_0(i\delta k, \omega) = i\delta k(\delta k - \theta)^2$. An inverse Laplace transform, by using the partial fraction expansion of (6a) (where the poles of the dispersion equation are $\delta k_1 = 0$ and $\delta k_{2,3} = \theta$), yields the well-known spectral relation for a prebunched low-gain FEL,

$$T_n(\omega) = \alpha_n L_w \frac{\sin(\bar{\theta}(\omega)/2)}{\bar{\theta}(\omega)/2}. \tag{15}$$

The spectral power density $|T_n(\omega)|^2 = (\alpha_n L_w)^2 \operatorname{sinc}^2(\bar{\theta}(\omega)/2)$ is just the spontaneous emission from uniform distributed shot noise $(|\tilde{n}_i(\omega)|^2 = \text{const.})$. The impulse response $h_n(\tau)$ is found by the inverse Fourier transform (13). In the low-gain limit, it has the form

$$h_n(t) = Ae^{-i\omega_0 t} \cdot \begin{cases} 1 & t_g < t < t_e \\ 0 & \text{otherwise} \end{cases} \tag{16}$$

where the resonant frequency ω_0 is defined by $\bar{\theta}(\omega_0) = 0$, and the amplitude $A = \alpha_n L_w/(t_e - t_g)$. The response $h_n(\tau)$

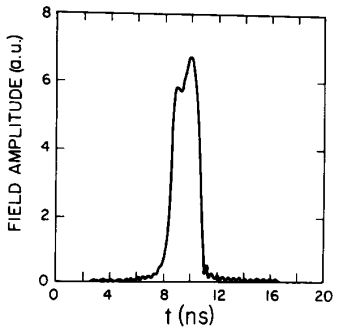

Fig. 8. The envelope of the FEL impulse response $h_n(t_2, t_1)$ computed from (13) for our experimental parameters, $t_1 = 6$ μs and $t = t_2 - t_1$.

from a current impulse at $t = 0$ has a square pulse envelope which starts at $t_g = L_w/V_g(\omega_0)$ and ends at $t_e = L_w/V_z$, where V_g is the group velocity, and t_g and t_e are the propagation times through the wiggler [32] of the radiation power and of a single electron, respectively. The impulse response pulsewidth is

$$\tau_s = t_e - t_g = \frac{L_w}{V_z} - \frac{L_w}{V_g}. \tag{17}$$

The time constant τ_s, the FEL slippage time, is related to the coherence time and to the linewidth in the low-gain limit, $\Delta\omega \cong \pi/\tau_s$. In free space, with $V_g = c$, one recovers the well-known expression $\Delta\omega = \omega_0/2N_W$.

The output field for an arbitrary time-dependent initial electron beam density $n_i(t)$ can be found from a convolution with the impulse response $h_n(\tau)$:

$$E_o(t, z = L_w) = \int_\tau n_i(t - \tau)h_n(\tau)\, d\tau. \tag{18}$$

Similar expressions can be derived which relate E_0 to the input field or to a velocity perturbation.

B. Linear Model of the FEL Oscillator

The radiation build-up process in an FEL oscillator incorporates processes of spontaneous emission and amplification. The oscillator consists of an FEL section and a cavity or a feedback loop, as shown schematically in Fig. 9. The FEL is modeled as a block with two inputs $\tilde{E}_i(\omega)$ and $\tilde{n}_i(\omega)$ and one output $\tilde{E}_o(\omega)$. The inputs and output have linear relations between them [given by (11a) and (11b), respectively].

The feedback loop, in a waveguide ring cavity geometry, is a lossy dispersive medium. The phase shift during one roundtrip in the cavity is

$$\phi_d(\omega) = \sqrt{\omega^2 - \omega_{co}^2}\,\frac{L_c}{c} \tag{19}$$

where L_c is the cavity length and $\omega_{co}/2\pi$ is the cutoff frequency of the TE_{10} mode. The waveguide dispersion curve and the beam line $\bar{\theta}(\omega, k_z, V_z) = 0$ are shown in Fig. 10. The intersection of these curves at points A and B determine the FEL operating conditions. As the electron energy decays, the slope of the beam mode line decreases, and the intersection points A and B converge to C. When the beam energy falls too low, no intersection is possible, and when the separation between the beam and waveguide becomes too large, no power is produced.

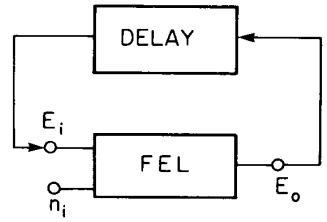

Fig. 9. A physical model of the FEL oscillator consisting of a time-dependent FEL and a dispersive feedback loop.

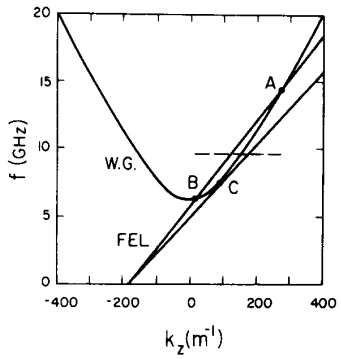

Fig. 10. The waveguide dispersion curve and the beam mode line ($\bar{\theta} = (\omega/V_z - k_z - k_w)L_w = 0$). The intersection points A and B determine the FEL resonance conditions. The slope of the beam mode line decays due to the electron energy droop. Point C determines the lowest electron velocity at which the FEL interaction can occur. The horizontal dashed line shows the filter band above 9.6 GHz.

The beam parameters for this experiment are slightly time dependent due to the slow variation in the electron beam energy (1). Fig. 11 shows the time dependence of the FEL resonance frequency f_0, the corresponding cavity round-trip time $t_d = L_c/V_g$, and the slippage time τ_s (17). The slippage time is much shorter than the round-trip time,

$$\tau_s \ll t_d \ll \tau_m \tag{20}$$

and thus we can apply a two-time-scale approach.

In order to find the impulse response of the FEL oscillator, we model it as a cascade of FEL blocks [33], as shown in Fig. 12. Each stage l in the cascade represents one round-trip period, which includes an FEL section [$FEL^{(l)}$] and a waveguide section [modeled as a delay element D_l, using (19)]. Each FEL block has two inputs: one for the electromagnetic wave E_i, and the other for the den-

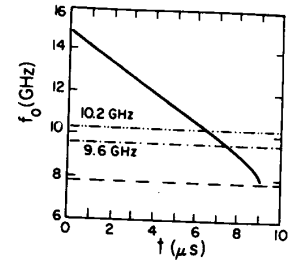

(a)

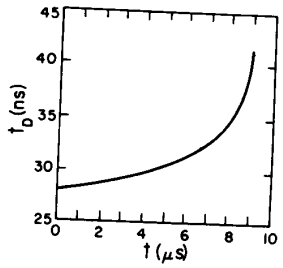

(b)

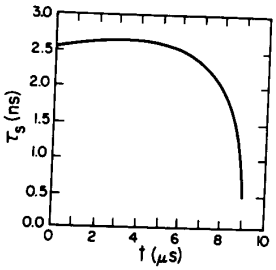

(c)

Fig. 11. The time dependence of (a) the FEL resonance frequency f_0 of point A (Fig. 10), (b) the 7.6 m cavity round-trip time $t_d = L_c/V_g$ of the instantaneous resonance frequency f_0, and (c) the slippage time τ_s (17).

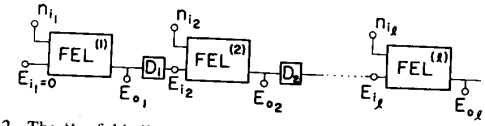

Fig. 12. The "unfolded" model of the FEL oscillator used for computation of the impulse response.

sity fluctuations n_i. By allowing each FEL block to have slightly different beam parameters, we can investigate the influence of the slow beam energy variation on the oscillator dynamics.

In the calculation, the FEL interaction is initiated by an initial input n_i, which represents a fluctuation in the beam density. This generates radiation emission at the output port E_o, which then propagates through the feedback loop to the input as an E_i, and is then reamplified in successive round-trips. The spiky behavior of the electron beam current described in the previous section suggests that the electron beam density fluctuations can be regarded as shot noise, namely

$$n_i(t) = n_0 + n_n \sum_i \delta(t - t_i) \tag{21}$$

where t_i are random points on the time axis distributed with a uniform density. Consequently, $\delta(t - t_i)$ are uncorrelated Poisson impulses. Such a shot noise model usually refers to fluctuations from single electrons. In this case, however, we apply it to the current spikes, shown in Fig. 5, as macroparticles.

For each FEL block, the linear transfer functions (11a) and (11b) define the spectral relations between the output $\tilde{E}_o(\omega)$ and the two independent inputs, $\tilde{E}_i(\omega)$ and $\tilde{n}_i(\omega)$, respectively, as

$$\tilde{E}_o(\omega)|_{n_i=0} = T_E^{(l)}(\omega)\tilde{E}_i(\omega), \qquad \tilde{E}_o(\omega)|_{E_i=0} = T_n^{(l)}(\omega)\tilde{n}_i(\omega) \tag{22a and (22b)}$$

where the transfer functions $T_E^{(l)}(\omega)$ and $T_n^{(l)}(\omega)$ are computed for the instantaneous FEL parameters at the lth round-trip.

The response of the FEL oscillator to a single density impulse $n_i(t) = n_0 + n_n\delta(t - t_1)$, is then given in the frequency domain by

$$\tilde{E}_o^{(l)}(\omega) = T_n^{(0)}(\omega) \cdot D^{(1)}(\omega) \cdot T_E^{(1)}(\omega) \cdot D^{(2)}(\omega) \cdots T_E^{(l)}. \tag{23}$$

Fig. 13(a) shows the spectral evolution of the signal in successive round-trips, as computed from (23). Fig. 13(b) shows the corresponding sweep of the center frequency of each micropulse due to the change in the accelerator voltage.

In the time domain, the FEL response at $t = t_2$ is given by an inverse Fourier transform of the cascade transfer function (23)

$$h_{osc}(t_2, t_1) = \frac{1}{2\pi}\int_\omega T_n^{(0)}(\omega) \prod_{l=1}^{m} T_E^{(l)}(\omega) \cdot \exp\left[i\omega t_2 - i(m-1)\phi_d(\omega)\right] d\omega \tag{24}$$

where $l = 0$ corresponds to $t = t_1$, and $l = m$ is the number of round-trips at $t = t_2$. The FEL response to a non-impulse electron density fluctuation $n_i(t) = n_0 + n_f(t)$, where $n_f(t)$ is much shorter than a round-trip time, is given, in general, by the convolution integral $E_o(t) = \int_{\tau=-\infty}^{t} h_{osc}(t, \tau) n_f(\tau)\, d\tau$.

We assume density fluctuations $n_i(t) = n_0 + \Sigma_j n_j\delta(t - t_j)$, with random amplitudes n_j and random appearance times t_j. Thus the output radiation $E_o(t)$ is a linear superposition of impulse responses $h_{osc}(t_2, t_j)$ for the random spikes $E_o(t_2) = \Sigma_j n_j h_{osc}(t_2, t_j)$. The output power is then

$$|E_o(t_2)|^2 = \left|\sum_j n_j h_{osc}(t_2, t_j)\right|^2 = \sum_j n_j^2 |h_{osc}(t_2, t_j)|^2. \tag{25}$$

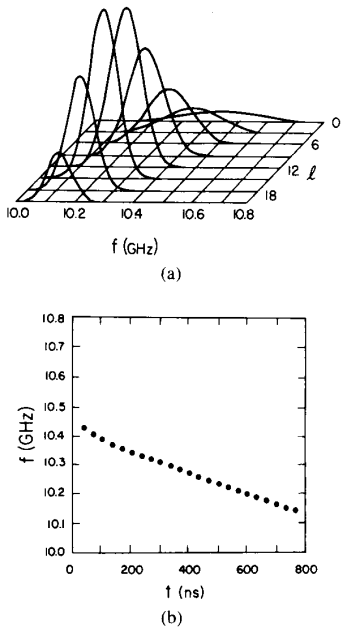

Fig. 13. (a) The spectral evolution of the FEL oscillator impulse response with a high-pass filter ($f > 9.6$ GHz) in the frequency domain, as computed from (23) for $t_1 = 6$ μs. (b) The center frequency at each round-trip.

The intensity of the impulse response $|h_{osc}(t_2, t_1)|^2$ with a high-pass filter ($f > 9.6$ GHz) is computed for the parameters of the experiment, and plotted as a function of time in Fig. 14. The theoretically calculated intensity shown in Fig. 14 resembles closely the observed bell-shaped macropulses shown in Figs. 4 and 6(a). In the computed FEL impulse response, the macropulse peak appears 507 ns after the current impulse, the period between two successive micropulses is ~33 ns, and the micropulsewidth is ~5 ns. These theoretical results are quite similar to the experimental measurements shown in Fig. 6. The spikes A′ and B′ [Fig. 6(b)] appear at $t_{A'} = 82$ ns and $t_{B'} = 317$ ns, respectively. The peak of macropulses A and B [Fig. 6(a)] appears at $t_A = 598$ ns and $t_B = 827$ ns, respectively. Hence, the time difference $t_A - t_{A'} = 516$ ns is close to the difference $t_B - t_{B'} = 510$ ns, and to the theoretical result, 507 ns. The observed signals in all our experimental runs are composed of partially overlapping macropulses with random amplitude and random appearance times, as would be expected from the theoretical model. The observed macropulses have the same structures as the computed $|h_{osc}(t_2, t_1)|^2$ shown in Fig. 14.

Fig. 15 shows the pulsewidth of each of the micropulses plotted in Fig. 14 and the pulsewidth of a micropulse in the absence of the FEL interaction (but including waveguide dispersion). It can be seen that, for these parameters, the tendency of waveguide dispersion to broaden the micropulse is counteracted somewhat by the gain and phase modification of the FEL.

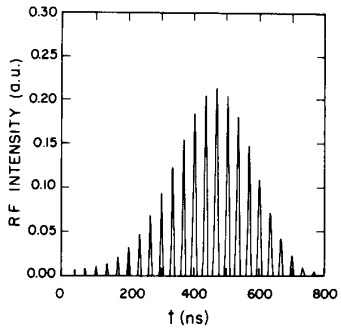

Fig. 14. The FEL impulse response intensity $|h_n(t_2, t_1)|^2$ in the time domain as computed from (24) for our experimental parameters.

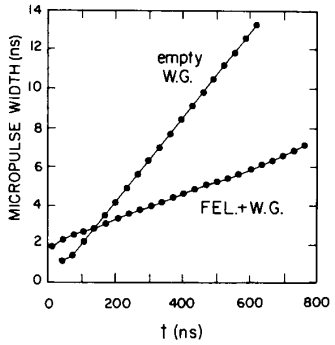

Fig. 15. The pulsewidth of the micropulses computed in Fig. 14 and their pulsewidth in the same waveguide ring cavity, but without the FEL interaction [$T_E(\omega) = 0$].

IV. Discussion

In this paper, we have identified a fundamental signal structure, the bell-shaped macropulse of Figs. 4 and 6(a), which is the underlying building block of the RF pulse near oscillation threshold. The experimental measurements of the time dependence of the macropulse are in agreement with a theoretical shot noise analysis of the FEL oscillator.

The agreement between experiment and theory is good but some underlying assumptions in the theory used to produce Fig. 14 cannot be verified experimentally with our present apparatus. In the experiment we observed a correlation between the macropulses [Fig. 6(a)] and spikes superposed on the electron beam current [Fig. 6(b)]. In the theoretical analysis, a random sequence of ideal impulses (21) serves as a model for the current spikes (Fig. 5). The observed spikes may have a pulsewidth as large as 1 ns, which is much longer than an RF period (0.1 ns). We assume however, without experimental verification, that these random spikes have a nonzero spectral content in the FEL frequency band. A nonuniformity in the spectral content of the spikes in the FEL frequency band causes some widening of the micropulses which can be easily

evaluated by a convolution integral, as in (18). The agreement between experiment and theory reinforces our conclusion that the radiation macropulse is generated by a current spike. In particular, in the example shown in Fig. 6(a) and (b) spike A′ excited macropulse A, and spike B′ excited macropulse B. In general, the shot noise in an FEL oscillator may be too small to be observed experimentally. This analysis suggests that the radiation power in the startup phase of a long pulse FEL oscillator is actually composed of a large number of such macropulses with uncorrelated random start-up times, as given by (25).

The bell-shaped envelope of the macropulse results from the beam voltage droop. This droop leads eventually to a violation of the FEL resonance conditions, and therefore to a reduction in the growth rate. At the peak of the macropulse, the FEL amplification equals the waveguide attenuation, and the net gain is zero. With a constant electron beam energy, the reamplification of the micropulse would continue until saturation.

It is evident that the micropulse periodicity should equal the round-trip time in the cavity, and this is confirmed by experiment and theory. The micropulse is subjected to the waveguide dispersion as well as the FEL phase shift, and its width and amplitude evolve as a function of time. The first micropulse in Fig. 14 is the instantaneous response of the FEL to the electron beam impulse. Its width is the FEL slippage time $\tau_s \cong 2.5$ ns. In following round-trips it slowly broadens to 5 ns near the macropulse peak, in agreement with the experiment [Fig. 6(a)]. This width is narrower than the pulsewidth which would result purely from waveguide dispersion, without the FEL interaction (Fig. 15). Hence, the FEL amplification and phase shift counteract the pulse broadening from waveguide dispersion.

Further experimental investigation of methods to control the micropulse and macropulse structure suggest themselves. For example, the macropulse could be initiated by an applied current perturbation, the electron beam energy droop can be adjusted to change the number of micropulses, and the dispersion may be adjusted to change the micropulse width. This may have practical applications, especially for electrostatic FEL's, as a method of producing sequences of tunable, high-power, short micropulses. A photocathode, for instance, may produce a sequence of short pulses, in addition to a dc electron beam, as in (2). In principle, with good control of the electron beam energy, the FEL may produce long macropulses with uniform amplitude.

References

[1] C. C. Cutler, "The regenerative pulse generator," in *Proc. IRE*, vol. 43, pp. 140–148, Feb. 1955.

[2] P. W. Smith, "The self-pulsing laser oscillator," *IEEE J. Quantum Electron.*, vol. QE-3, pp. 627–635, 1967.

[3] ——, "Mode locking of lasers," in *Proc. IEEE*, vol. 58, pp. 1342–1357, 1970; for recent studies on ultrafast laser phenomena, see the Special Issue of *IEEE J. Quantum Electron.*, vol. 25, Sept. 1989.

[4] L. F. Mollenauer and R. H. Stollen, "The soliton laser," *Opt. Lett.*, vol. 9, pp. 13–15, 1984.

[5] R. W. Warren, B. E. Newnam, and J. C. Goldstein, "Raman spectra and the Los Alamos free electron laser," *IEEE J. Quantum Electron.*, vol. QE-21, pp. 882–888, 1985.

[6] J. Masud, T. C. Marshall, S. P. Schlesinger, and F. G. Yee, "Gain measurements from start-up and spectrum of a Raman free-electron-laser oscillator," *Phys. Rev. Lett.*, vol. 56, pp. 1567–1570, 1986.

[7] W. B. Colson, "The trapped particle instability in free electron laser oscillators and amplifiers," *Nucl. Instrum. Methods Phys. Res.*, vol. A250, pp. 168–175, 1986.

[8] J. C. Goldstein, B. W. Newman, R. W. Warren, and R. L. Sheffield, "Comparison of the results of theoretical calculations with the Los Alamos free electron laser oscillator experiment," *Nucl. Instrum. Methods Phys. Res.*, vol. A250, pp. 4–11, 1986.

[9] B. A. Richman, J. M. J. Madey, and E. Szarmes, "First observation of spiking behavior in the time domain in a free electron laser," *Phys. Rev. Lett.*, vol. 63, pp. 1682–1684, 1989.

[10] J. W. Dodd and T. C. Marshall, "Spiking radiation in the Columbia free electron laser," *Nucl. Instrum. Methods Phys. Res.*, vol. A296, pp. 4–8, 1990.

[11] Y. Kawamura, K. Toyoda, and M. Kawai, "Observation of periodic short pulse trains in free electron laser oscillations," *Appl. Phys. Lett.*, vol. 51, pp. 795–797, 1987.

[12] M. N. Rosenbluth, H. V. Wong, and B. N. Moore, "Sideband instabilities in free electron lasers," *Phys. Fluids*, vol. B2, pp. 1635–1653, 1990; see also N. M. Kroll and M. N. Rosenbluth, in *Physics and Quantum Electronics*. Reading, MA: Addison-Wesley, 1980, vol. 7, p. 147.

[13] E. Jerby, G. Bekefi, and J. S. Wurtele, "Observations of periodic intensity bursts during the start-up phase of a free-electron laser oscillator," *Phys. Rev. Lett.*, vol. 66, pp. 2068–2071, 1991.

[14] H. A. Haus, "Noise in free-electron laser amplifier," *IEEE J. Quantum Electron.*, vol. QE-17, pp. 1427–1431, 1981.

[15] P. Sprangle, C. M. Tang, and I. Bernstein, "Evolution of spontaneous and coherent radiation in the free-electron laser oscillator," *Phys. Rev. A*, vol. 28, pp. 2300–2309, 1983.

[16] K. J. Kim, "Three-dimensional analysis of coherent amplification and self-amplified spontaneous emission in free-electron lasers," *Phys. Rev. Lett.*, vol. 57, pp. 1871–1874, 1986.

[17] I. Schnitzer and A. Gover, "Prebunched FEL in various operating gain regimes," *Nucl. Instrum. Methods*, vol. A237, pp. 124–140, 1985.

[18] J. S. Wurtele, G. Bekefi, R. Chu, and K. Xu, "Prebunching in a collective Raman free-electron laser amplifier," *Phys. Fluids*, vol. B2, pp. 401–406, 1990.

[19] B. Bonifacio, B. W. J. McNeil, and P. Pierini, "Superradiance in the high-gain free-electron laser," *Phys. Rev. A*, vol. 40, pp. 4467–4475, 1989.

[20] S. Y. Cai, J. Cao, and A. Bhattacharjee, "Linear theory of superradiance in a free-electron laser," *Phys. Rev. A*, vol. 42, pp. 4120–4126, 1990.

[21] J. C. Gallardo, L. Elias, G. Datoli, and A. Renieri, "Instability in a multimode free electron laser: effects of electron energy drift," *Phys. Rev. A*, vol. 34, pp. 3088–3100, 1986.

[22] T. M. Antonsen Jr. and B. Levush, "Mode competition and control in free-electron laser oscillator," *Phys. Rev. Lett.*, vol. 62, pp. 1488–1491, 1989.

[23] D. Oepts and W. B. Colson, "Phase locking in an infrared short-pulse free-electron laser," *IEEE J. Quantum Electron.*, vol. 26, pp. 723–730, 1990.

[24] J. Fajans, G. Bekefi, Y. Z. Yin, and B. Lax, "Spectral measurements from a tunable, Raman, free-electron laser," *Phys. Rev. Lett.*, vol. 53, pp. 246–249, 1984.

[25] F. Hartemann, K. Xu, and G. Bekefi, "Generation of short pulses of coherent electromagnetic radiation in free electron laser amplifier," *IEEE J. Quantum Electron.*, vol. 24, pp. 105–112, 1988.

[26] K. Xu, G. Bekefi, and C. Leibovitch, "Observations of field profile modifications in Raman free-electron laser amplifier," *Phys. Fluids*, vol. B1, pp. 2066–2072, 1989.

[27] A. Gover and P. Sprangle, "A unified theory of magnetic bremsstrahlung, electrostatic bremsstrahlung, Compton–Raman scattering, and Cerenkov–Smith–Purcell free-electron lasers," *IEEE J. Quantum Electron.*, vol. QE-17, pp. 1196–1215, 1981.

[28] E. Jerby and A. Gover, "Investigation of the gain regimes and gain parameters of the free electron laser dispersion equation," *IEEE J. Quantum Electron.*, vol. QE-21, pp. 1041–1058, 1985.
[29] E. Jerby, "Angular steering of the free-electron laser far-field radiation beam," *Phys. Rev. A*, vol. 41, pp. 3804–3812, 1990.
[30] J. R. Pierce, *Traveling Wave Tubes*. Princeton, NJ: Van-Nostrand, 1950.
[31] "Notes on the partial coherence of the free electron laser," E. Jerby, Microwave Lab. Note 90/3, Tel Aviv University, 1990.
[32] C. Brau, *Free Electron Lasers*. New York: Academic, 1990, ch. 3.
[33] A. Gover, H. Freund, V. L. Granatstein, J. S. McAdoo, and C. M. Tang, "Basic design considerations for FELs driven by electron beams from RF accelerators," NRL Rep. 8747; also in *Infrared and millimeter waves*, vol. 11, K. J. Button, Ed. New York: Academic, 1984, ch. 8.

Eli Jerby was born in Israel in 1957. He received the B.Sc., M.Sc., and Ph.D. degrees in electrical engineering from Tel Aviv University, Israel, in 1979, 1980, and 1989, respectively.

He worked at M.I.T. as a post-doctoral fellow where he was involved in theoretical and experimental studies of FEL oscillators. Currently, he is a lecturer with the Faculty of Engineering, Tel Aviv University, where he teaches courses on microwave engineering and conducts research on hybrid free-electron laser devices.

George Bekefi, for a photograph and biography, see this issue, p. 2507.

Jonathan S. Wurtele, photograph and biography not available at the time of publication.